Image-assisted aerial LiDAR completion with morphology-guided gaussian splatting

Siyuan Zou [1], Yongjun Zhang [2], Zhiwei Li [1], Hongbo Pan [1*], Xinyi Liu [2], Haojun Tang [1], Hai Kan [3]

[1] School of Geoscience and Info-Physics, Central South University, Changsha, China - zousiyuan@163.com, zwli@csu.edu.cn, hongbopan@csu.edu.cn, 3279179450@qq.com

[2] School of Remote Sensing and Information Engineering, Wuhan University, Wuhan, China - zhangyj@whu.edu.cn, liuxy0319@whu.edu.cn

[3] School of Resource and Environmental Sciences, Wuhan University, Wuhan, China - 2025282050209@whu.edu.cn

Keywords: LiDAR, Gaussian Splatting, Point Cloud Densification, Multi-Modal Data Fusion, 3D Modeling.

1. Introduction

Airborne LiDAR offers high geometric accuracy and efficient wide-area coverage, and has been widely used in applications such as urban 3D reconstruction, forestry inventory, topographic mapping, and powerline extraction (Ye et al., 2020; Han et al., 2024; Yin et al., 2024). However, due to near-nadir acquisition geometry and occlusions, vertical structures such as building façades are often under-sampled, resulting in large voids in the point cloud (Domínguez et al., 2025). Traditional geometric hole-filling methods, including Moving Least Squares, Poisson surface reconstruction, and mesh repair, are effective for small gaps, but they often suffer from over-smoothing, structural distortion, and topological discontinuities when applied to large-scale missing regions.

Meanwhile, multi-view imagery can recover continuous surfaces through dense matching or Gaussian Splatting, but the reconstruction quality still depends heavily on the completeness of the initial geometry (Zhang et al., 2022; Kerbl et al., 2023). When the initial triangulated points or geometric priors are incomplete, façade regions remain prone to fragmentation and noise (Zhang et al., 2025). This paper proposes an image-assisted LiDAR completion framework that models LiDAR completion as continuous surface reconstruction with explicit Gaussians. Through anisotropic Gaussian initialization and tangent-plane-guided densification, the method preserves façade geometry and improves the completeness and accuracy of LiDAR-image fusion reconstruction.

2. Methodology

This study proposes an image-assisted LiDAR completion framework based on morphology-guided Gaussian ellipsoids, as illustrated in Figure 1. First, LiDAR point clouds and multi-view images are georeferenced and centroid-normalized in a unified coordinate system. Then, LiDAR-guided Gaussian ellipsoid initialization introduces geometric priors for anisotropic modeling. Finally, tangent-plane-guided Gaussian densification generates additional Gaussian points to improve local details and structural continuity, producing a more complete and accurate 3D Gaussian representation.

2.1 Georeferencing of LiDAR Point Clouds and Multi-view Images

A GPS-constrained aerial triangulation was performed to estimate image exterior orientations. The resulting triangulation point cloud, camera poses, and LiDAR point cloud were transformed into a common Earth-Centered Earth-Fixed coordinate system and then jointly centroid-normalized to ensure spatial consistency and improve numerical stability for subsequent Gaussian Splatting.

2.2 LiDAR-guided Gaussian Ellipsoid Initialization

To enhance the geometric consistency of 2D Gaussian Splatting (2DGS, Huang et al., 2024), laser point cloud priors are introduced for geometry-aware initialization. For each laser point $P_i = (x_i, y_i, z_i)$ with color $C_i = (r_i, g_i, b_i)$,the Gaussian center and spherical harmonics (SH) coefficients are initialized as

$$\mu_i = P_i, c_i^{(0)} = C_i \tag{1}$$

The surface normal n_i is estimated from the local covariance matrix

$$\sum_i = \frac{1}{k}\sum_{j=1}^{k}(P_j - \overline{P_i})(P_j - \overline{P_i})^{\mathrm{T}} \tag{2}$$

and the eigenvector of the smallest eigenvalue defines the ellipsoid orientation.

To adapt the Gaussian scale to the local geometry, the distances to neighboring points are used to update the first two scale parameters of each Gaussian, reflecting the local spatial distribution. The third scale is set to zero, constraining the ellipsoid along the normal direction. The opacity of each Gaussian is initialized to a relatively high value to emphasize the contribution of reliable laser observations during early optimization.

2.3 Tangent-Plane Guided Gaussian Densification

To reconstruct the void regions in the LiDAR data, a gradient-guided densification strategy is applied. Gaussians with gradient magnitude $\| g_i \| \geq g_{th}$ and sufficiently small scale relative to the scene extent are selected as parents, optionally filtered by planar confidence $c_i \geq c_{th}$. For each parent, tangent-plane oriented clones are generated along the local basis (t_u, t_v) derived from either LiDAR normals or the parent rotation quaternion q_i . Child positions are offset based on parent scale and offset factor:

$$x_{child} = x_{parent} + \delta_u t_u + \delta_v t_v \tag{3}$$

where δ_u , δ_v are scaled offsets. Child parameters—including log-scale, rotation, SH color coefficients, and opacity—are inherited from the parent, with scale and opacity optionally attenuated. The opacity is set to

$$\alpha_{child} = \alpha_{parent} \cdot \beta, \beta < 1 \tag{4}$$

ensuring moderate contribution of new Gaussians. All children are concatenated with existing Gaussians and registered for optimization, increasing density while preserving local geometry and feature continuity.

3. Experiments and Results

The proposed approach was validated using airborne LiDAR data and co-registered RGB imagery acquired by the DJI Zenmuse L1. The test areas mainly include two representative types of buildings—houses with eaves and houses without eaves—which present distinct visibility conditions for LiDAR and imagery. For houses without eaves, the roofs and façades are clearly visible in the images, whereas the LiDAR points are relatively sparse or even missing. In contrast, for houses with eaves, both LiDAR and imagery suffer from occlusion in the areas beneath the eaves.

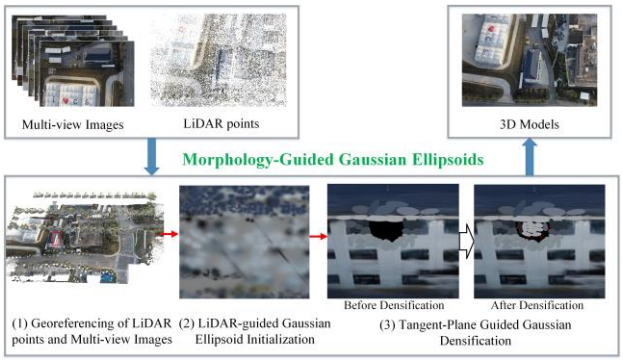

Figure 1. The overall workflow of the proposed method

(a) AT-guided Gaussian Splatting reconstruction (b) LiDAR-guided Gaussian Splatting reconstruction

Figure 2. Comparison of 3D reconstruction results

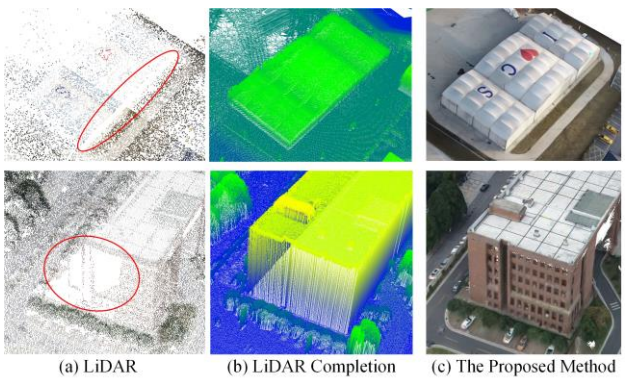

Figure 3. Comparison of LiDAR Points and 3D model.

Figure 2 presents a comparison of 3D reconstruction results. In Figure 2(a), the AT-guided Gaussian Splatting reconstruction shows large missing regions on walls and pillars, resulting in incomplete surface geometry. In contrast, Figure 2(b) demonstrates that the LiDAR-guided reconstruction effectively recovers wall and pillar details. This comparison highlights the clear advantage of LiDAR guidance in improving surface completeness and structural fidelity.

Figure 3 presents a comparison between the LiDAR points and 3D model produced by LiDAR completion and the proposed method. In Figure 3(a), the LiDAR data shows noticeable gaps on building façades due to incomplete laser returns. In Figure 3(b), LiDAR completion fills all point-cloud gaps. However, in large missing regions, the façades remain coarse, and errors occur in perforated or hollow areas. In Figure 3(c), the dense reconstruction generated by our method effectively fills these missing regions and significantly increases point density. Small unrecovered areas remain beneath the eaves because they are invisible in the aerial images. Overall, this comparison demonstrates that the image-assisted LiDAR completion approach substantially enhances LiDAR completeness and density while maintaining geometric consistency.

To quantitatively evaluate reconstruction accuracy, denser and more complete point clouds were used as reference data to assess the precision of the reconstructed models. Three evaluation metrics—Precision (P), Recall (R), and F1-score (F1)—were employed to measure geometric accuracy and completeness. Their formulations are defined as:

$$P = \frac{TP}{TP + FP}, R = \frac{TP}{TP + FN}, F1 = \frac{2PR}{P + R} \quad (5)$$

where TP, FP and FN represent the numbers of true positive, false positive, and false negative points, respectively, determined by a distance threshold (1 meter) between reconstructed and reference points. Experiments on houses with and without eaves show that the proposed method consistently outperforms 2DGS (Table 1), with F1-score gains of 8.3% and 7.8%, demonstrating improved geometric completeness and robustness.

Table 1 Reconstruction Accuracy Comparison (Unit:%)

Method	houses without eaves			houses with eaves		
	P ↑	R ↑	F1 ↑	P ↑	R ↑	F1 ↑
2DGS	77.8	84.7	81.1	70.5	62.6	66.3
Our	**83.7**	**92.3**	**87.8**	**75.1**	**68.1**	**71.5**

4. Conclusion

This paper presents an image-assisted LiDAR completion method for airborne LiDAR-camera reconstruction. By introducing LiDAR-guided anisotropic Gaussian initialization and tangent-plane-guided densification, the method improves façade completeness, point density, and reconstruction accuracy while preserving geometric consistency. Experimental results on real airborne datasets demonstrate its effectiveness for accurate and structurally consistent surface reconstruction.

References

Domínguez, E.M., Brotzer, P., Casalini, E., Small, D., 2025. Mapping Urban Areas and Infrastructure Through Fusion of Airborne SAR 3-D Images: A Comparative Study With ALS Sensors. IEEE J. Sel. Top. Appl. Earth Obs. Remote Sens. 18, 6164–6181.

Han, X., Liu, C., Zhou, Y., Tan, K., Dong, Z., Yang, B., 2024. WHU-Urban3D: An urban scene LiDAR point cloud dataset for semantic instance segmentation. ISPRS J. Photogramm. Remote Sens. 209, 500–513.

Huang, B., Yu, Z., Chen, A., Geiger, A., Gao, S., 2024a. 2D Gaussian Splatting for Geometrically Accurate Radiance Fields. Presented at the ACM SIGGRAPH 2024, pp. 1–11.

Kerbl, B., Kopanas, G., Leimkühler, T., Drettakis, G., 2023. 3D Gaussian Splatting for Real-Time Radiance Field Rendering.

Ye, Z., Xu, Y., Huang, R., Tong, X., Li, X., Liu, X., Luan, K., Hoegner, L., Stilla, U., 2020. LASDU: A Large-Scale Aerial LiDAR Dataset for Semantic Labeling in Dense Urban Areas. ISPRS Int. J. Geo-Inf. 9, 450.

Yin, D., Wang, L., Lu, Y., Shi, C., 2024. Mangrove tree height growth monitoring from multi-temporal UAV-LiDAR. Remote Sens. Environ. 303, 114002.

Zhang, Y., Jiang, G., Li, M., Feng, G., 2025. The 3D Gaussian Splatting SLAM System for Dynamic Scenes Based on LiDAR Point Clouds and Vision Fusion. Appl. Sci. 15, 4190.

Zhang, Y., Zou, S., Liu, X., Huang, X., Wan, Y., Yao, Y., 2022. LiDAR-guided stereo matching with a spatial consistency constraint. ISPRS J. Photogramm. Remote Sens. 183, 164–177.